IRSTI 29.03.30

Investigation of the low-temperature cyclohexane oxidation

M. Abbasi and N.A. Slavinskaya*

Institute of Combustion Technology, German Aerospace Center (DLR), Stuttgart, Germany
*e-mail: Nadja.Slavinskaya@dlr.de

The existence or non-existence of the negative temperature coefficient (NTC) region in cyclo-hexane (cyC_6H_{12}) oxidation is still an open question in the literature. This paper addresses this issue by presenting the rapid compression machine (RCM) and shock tube (ST) data and a consistent model to predict ignition delay times in agreement with experimental data. To this end, a semi-detailed chemical kinetic mechanism has been updated and improved to study the cyclohexane combustion at both low- and high-temperatures including polyromantic molecule (PAH) formation. The reaction mechanism is based on the 20 reaction classes; two of those were newly included in the model: cyclohexenyl peroxy formation and isomerization of hydroperoxy peroxy radical. For the main reaction classes, uncertainty boundaries of the rate coefficients have been evaluated. The NTC behavior observed in the RCM experiments was not detected in the ST measurements and in simulations performed with the developed model. The simulations performed with other literature models revealed that reaction models, which described the NTC region fixed in the RCM experiments, were unable to reproduce accurately the shock tube data. It is shown, that the cyC_6H_{12} oxidation chemistry is controlled by competition between three main reaction pathways over the full temperature interval. The developed model describes successfully laminar flame speed data and species profiles from burner-stabilized premixed flames.

Key words: cyclohexane, oxidation, polyaromatics, ignition, NTC.
PACS numbers: 07.20.Mc; 82.40.−g.

1 Introduction

Cycloalkanes (naphthenes) are an important chemical class of hydrocarbons found in conventional fuel mixtures like kerosene and diesel. They can affect the ignition quality of the fuel and can potentially raise soot emission levels due to their cyclic shapes. Therefore, the kinetic investigation of cyclohexane as the basic naphthene used in the models of commercial fuels has a great importance.

Table S1 in *Supplement-1* summarizes the main existing numerical investigations of the cyC_6H_{12} chemistry [1-10] accomplished with the experimental data [11-22] details used for the model validations. Despite of numerous investigations, up to now the published reaction models demonstrate significant discrepancies in the kinetic parameters and results. Thus the ignition delay time measurements performed in RCM [11, 17] and ST [16, 22] report contradictive information: NTC region observed in RCM was not detected in the ST experiments. To our knowledge, the published models were validated mostly on the data followed from RCM. An exception is reaction mechanism developed by Serinyel et al. [10] which was tested also on the ST low-temperature data of Daley et al. [16]. The indicated significant discrepancy between experiment and simulations was not analyzed in the study [10].

The main objective of this study is to revise and update the reaction pathways and rate coefficients of important reactions in the DLR kinetic model [23] and to establish the uncertainty quantified reaction mechanism of the cyC_6H_{12} oxidation with reasonable size to study the whole reactivity range. This model will be the base for the further extension to substituted, mono- and polycyclic napthenes. The investigation of the difference in the low-temperature data obtained in RCM and ST experiments is in the

focus of the present paper. By simulations of the experimental data with the updated mechanism and conducting chemical kinetic analyses the controlling reaction pathways responsible for autoignition at the lower temperature are identified and discussed.

The kinetic model was tested on the experimental data obtained in laminar flames. It delivers realistic predictions for cyclohexane combustion and due to its compactness meets the requirements of CFD simulations for technical combustion system.

Kinetic Model

The presented cyclohexane oxidation kinetic mechanism is a significant update of the model developed earlier in DLR [23]. The new model is based on the most recent C_0-C_3 chemistry studied by Slavinskaya et al. [24, 25, 26] and includes the PAH sub-model up to 5-ringed molecules.

Thermodynamic properties for several cyclic species were newly estimated and revised based on Benson's additivity approach including cyclic and bicyclic ring correction groups, reported in [27] , Table S2. The species transport properties were approximated using the group contribution algorithm of Joback et al. [28]. The full reaction mechanism, thermodynamic and transport data are provided in supplemental files (*Supplement_Mech, Supplement_therm, Supplement_trandat*).

Simulation of the experimental data was performed using the SENKIN and PREMIX packages of CHEMKIN II [29]. To model the ignition delay data obtained in RCM with the pressure profile, the chemical work bench (CWB) packages [30] have been used. For simulations of the ignition delay times measured in RCM, it was assumed that no reaction occurs during the compression stroke, heat losses are negligible and the constant volume assumption can be used. Simulations performed with the pressure profile shown the negligible effect of the pressure gradients on results. Constant-volume, homogeneous, and adiabatic conditions have been used to model the shock tube experiments.

2.1 High Temperature Sub-Mechanism

After sensitivity and rate of production analysis only 6 main reaction classes marked in Figure 1 were found to be important for high-temperature:

1. Unimolecular fuel decomposition, ring opening;
2. H-atom abstraction by O, H, OH, CH_3, CH_3O, C_2H_3, C_2H_5, O_2 leading to cycloalkyl radical, cyC_6H_{11};
3. Isomerization of cyC_6H_{11}, ring opening/β-scission of cyclic radicals;
4. Decomposition of unsaturated cyclic molecules;
5. Cascading dehydrogenation of cyC_6H_{11} (H-abstraction) leading to benzene (A1,C_6H_6);
6. cyC_6H_8 reactions to form, benzene

The kinetic rate parameters for reactions of type 1, as well as the further sequential unimolecular decompositions and β-scission reactions follow from the published literature reaction models [1, 3, 5, 6, 31, 32] . For cascading dehydrogenation steps, $cyC_6H_{11}\rightarrow cyC_6H_{10}\rightarrow cyC_6H_9\rightarrow\ldots\rightarrow$A1, due to the lack and high uncertainty level of data, the reaction coefficients were estimated, applying empirical rules proposed in [33] to evaluate the activation energy for H-abstraction reactions, *Supplement-2*. The pre-exponential factors were estimated based on the collision theory [34] using the numerical algorithm proposed in Cherny et al. [35].

2.2 Low Temperature Sub-Mechanism

Generally, cyclohexane exhibits low-temperature chemistry very similar to that of normal alkanes [36] with some cyclohexane specific reaction pathways like cyclohexanone and bicyclic ether formation. It was found [8, 9, 37] that the presence of the cyclic ring contributes to the activation energy barriers for some low-temperature reactions. It was considered at the rate coefficients evaluations, which were adopted mostly from investigations [4, 8, 9, 10, 32, 38, 39, 40] after the uncertainty analysis.

The main 14 reaction types were finally included in the scheme, Figure 2:

1. The O_2 addition to alkyl radical;
2. Isomerization of cyclic peroxy to hydroperoxy radical;
3. Decomposition $cyC_6H_{10}OOH\bullet$ radicals to cyclohexene and HO_2;
4. Decomposition $cyC_6H_{10}OOH\bullet$ radicals via ring opening to smaller species and OH radical;
5. Decomposition of $cyC_6H_{10}OOH\bullet$ and formation of cyclohexanone ($cyC_6H_{10}Od$) and 3 bicyclic ethers ($cyC_6H_{10}Oa,b,c$);
6. O_2 addition to $cyC_6H_{10}OOH\bullet$ with formation of $O_2QOOH\bullet$ type radicals;
7. Isomerization of $cyOOC_6H_{10}OOH$ to $cyC_6H_9(OOH)_2$
8. Decomposition of $cyOOC_6H_{10}OOH$ and $cyC_6H_9(OOH)_2$ to cyclic ketohydroperoxides ($cyOC_6H_9OOH$) and OH;
9. H-atom abstraction-cyclic ethers & cyclohexanone;
10. Decomposition of cyC_6H_9O;
11. Decomposition of $cyOC_6H_9OOH$ via ring opening;

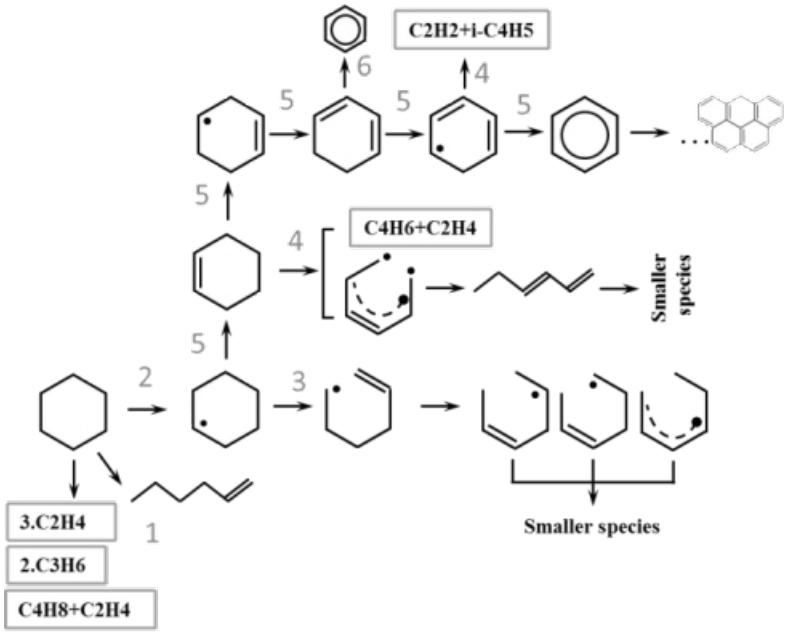

Figure 1 – Principal scheme of the high temperature oxidation of cyC_6H_{12}

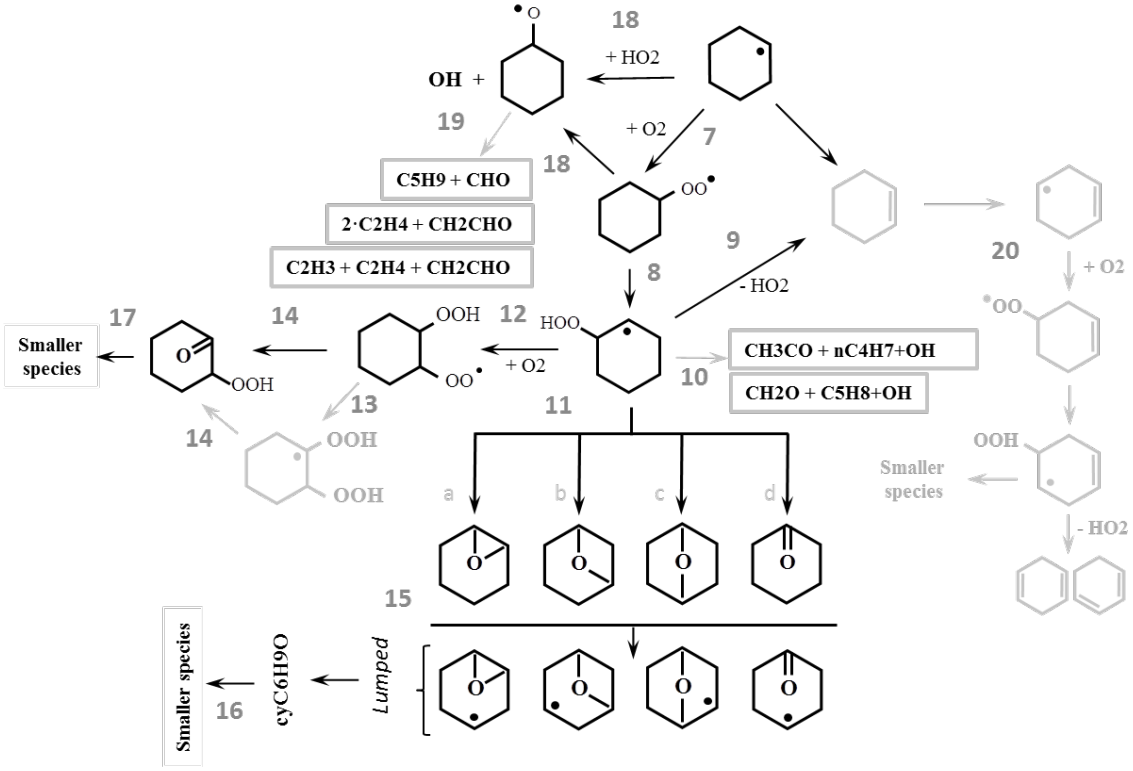

Figure 2 – Principal scheme of the low-temperature oxidation of cyC_6H_{12} with their new extensions (grey)

12. Formation of $cyC_6H_{11}O\bullet$ from $cyC_6H_{11}OO$ and cyC_6H_{11};

13. Decomposition of $cyC_6H_{11}O\bullet$ via ring opening;

14. The O_2 addition to cyC_6H_9.

The low-temperature reaction pathways earlier studied in [23] were revised and extended with the cyclohexenyl peroxy formation and isomerization of hydroperoxy peroxy radical, $cyOOC_6H_{10}OOH$, through the internal hydrogen transfer yielding more stable $cyC_6H_9(OOH)_2$ (type 13, Figure 2). The possible isomers of $cyC_6H_9(OOH)_2$ were grouped in a single lumped component, which dissociates into cyclic ketohydroperoxide and OH. This step was included in the scheme to multiply the chain propagation steps, and to increase the concentrations of less reactive HO_2 and cyclohexanone radicals (through the $cyOC_6H_9OOH$ decomposition) in the intermediate temperature zone.

Cyclohexene is mostly produced at the cascading cyclohexane dehydrogenation and at the HO_2 elimination from cyclohexylperoxy radical. Further that decomposes to cyclohexenyl, cyC_6H_9, which in turn after oxygen addition prolongs the low-temperature cyclohexene oxidation path competitive with the low-temperature hexyl oxidation. These two new added pathways, globally represented in the scheme in Figure 2, were not previously considered in detail in current understanding of low-temperature chemistry of cyclohexane. The related rate constants were evaluated as analogous to those for peroxy radicals, ROO and OOQOOH, applying cyclo-specific rate modification rules studied intensively by [8, 9, 37] (*Supplement_mech*).

2.3 Uncertainty Analysis

The upper f_u and lower f_l uncertainty boundaries of reaction rate coefficients have been evaluated through the statistical analysis of the literature data applying the non-linear weighted least squares method and its numeric realization FUMILI [41].

$$f_u(T) = log\frac{k_{upper}(T)}{k_0(T)}$$
$$f_l(T) = log\frac{k_0(T)}{k_{low}(T)} \quad (1)$$

here, k_0 is the nominal rate value, k_{low} and k_{upper} are lower and upper rate values from the dataset under consideration. This statistical assessment has been carried out, if a number of data sources exceeded 3. Table 1 summarises the clculated uncertainties. Detailed explanations about the applied method are provided in *Supplement-2*. These evaluated uncertainty intervals have been considered in the model improvement procedure. Table S3 reports parameters of the rate coefficients before and after modifications, and estimated uncertainty margins.

Table 1 – The lower and upper uncertainty factors of the rate coefficients of main reaction types

Reaction*	Type	$f_l(T)$	$f_u(T)$
$cyC_6H_{12} \rightarrow 3C_2H_4$	DE (1)	2.33-3.78	0.92-2.37
$cyC_6H_{12} \leftrightarrows aC_6H_{12}$	RN (1)	5.88-6.20	4.85-5.17
$cyC_6H_{12}+O_2 \leftrightarrows cyC_6H_{11} + HO_2$	HABS,INT (2)	2.47-2.65	2.44-2.62
$cyC_6H_{11} \leftrightarrows C_6H_{11}$	RN (3)	2.82-2.92	2.71-2.80
$cyC_6H_{11} \leftrightarrows cyC_6H_{10} + H$	DE (5)	3.38-3.57	3.07-3.26
$cyC_6H_{11}+O_2 \leftrightarrows cyC_6H_{10} + HO_2$	HABS (5)	1.68-1.79	1.66-1.77
$cyC_6H_{10} \leftrightarrows cyC_6H_9 + H$	DE (5)	3.11-3.21	2.82-2.92
$cyC_6H_{11}+O_2 \leftrightarrows cyC_6H_{11}OO$	ADD (7)	6.40-6.83	6.1-6.58
$cyC_6H_{11}OO \leftrightarrows cyC_6H_{10}OOH$	ISM (8)	3.34-3.85	3.31-3.82
$cyC_6H_{10}OOH \rightarrow CH_2O + C_5H_8 + OH$	BSC, RN (10)	4.28-4.73	3.33-3.78
$cyC_6H_{10}OOH \leftrightarrows OH+cyC_6H_{10}Oa$	DE-OH (11)	3.00-3.14	2.84-2.99
$cyOOC_6H_{10}OOH \leftrightarrows OH+ cyOC_6H_9OOH$	DE-OH (14)	2.87-2.92	2.77-2.82
$cyC_6H_{10}Oa+OH \leftrightarrows cyC_6H_9O+H_2O$	HABS (15)	0.89-0.93	0.88-0.93
$cyC_6H_{11}O \rightarrow CH_2CHO + 2C_2H_4$	DE,RN (19)	2.65-286	2.56-2.75

Abbreviations:
DE: Decomposition INT: Initiation HABS: H atom Abstraction RN: Ring-opening BSC: β- Scission ADD: Addition ISM: Isomerization DE-OH: Decomposition to release OH

3 Results and discussion

The performance of the current cyclohexane model was validated and optimized based on various types of experimental data [10-22], Table S4.

3.1 Ignition delay time

Rapid compression machine

The simulations of experimental data obtained in RCMs of [11, 17] revealed that unlike the mechanisms developed by Silke et al. [8] and Serinyel et al. [10], the studied model did not reproduce two stage ignition with NTC behavior.

The additive channels did not improve significantly trends in the ignition simulations, Figure 3, but made faster the ignition at T<800K: the additive O–OH bonds increase the number of OH radicals.

Generally, occurrence of NTC behavior in the hydrocarbon ignition is mainly controlled by the equilibrium of $cyC_6H_{11}+O_2 \leftrightarrows cyC_6H_{11}OO$. The shift in the reaction equilibrium to the $cyC_6H_{11}OO$ production favors the transition of the overall oxidation chemistry to the low-temperature kinetics. According to the used thermochemistry, the cyclohexyl peroxide production dominates on the whole investigated temperatures interval supporting the low-temperature mechanism of the small radical production. The temperature increase favors the reaction types 1-6 and reduces the peroxy radical concentration. That decreases the role of low-temperature reactions, but does not make it negligible. As a consequence, the region of gradient change (RGC) in the cyclohexane ignition behavior can be occurred as a response of the competition between low-and high-temperature reaction pathways. Instead the NTC regime, the smoothed conversion of the high-temperature oxidation to the low-temperature (an increase of reactivity with temperature decrease) is formed. The simulations of ignition delay data obtained in shock tubes support this conclusion.

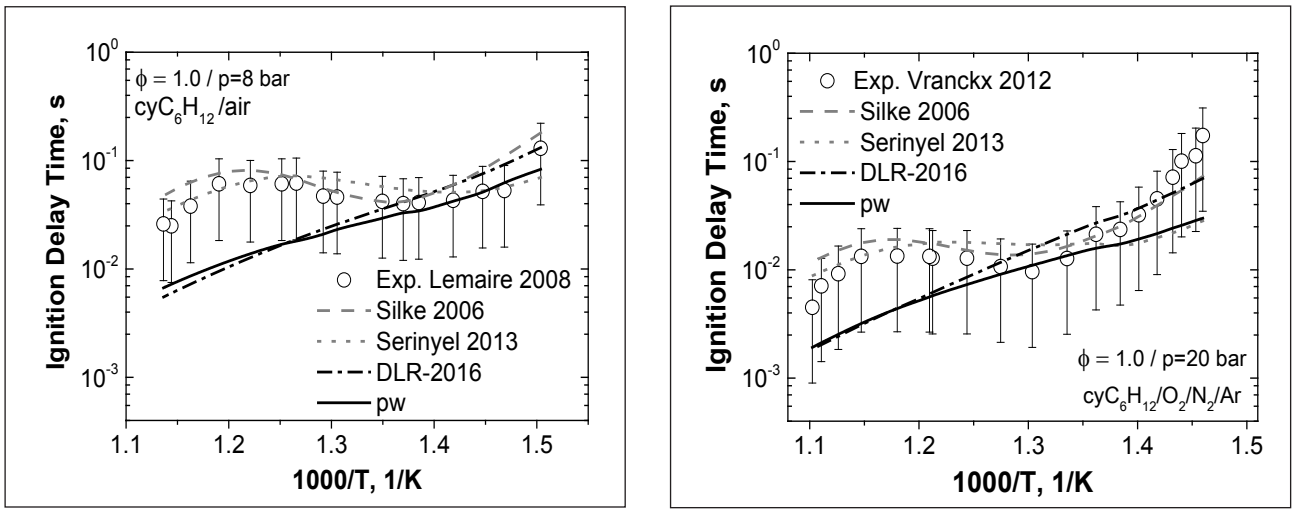

(a) (b)

Figure 3 – Cyclohexane ignition delay time from RCM experiments: a) p=8bar [11] b) p=20bar [17], versus simulations [8, 10], present work (pw)

Shock tube

The shock tube experiments performed by Daley et al. [16] and recently by Naumann et al. [22], Fig.4 and 5, do not demonstrate the NTC region, but the clear increase in reactivity with the temperature decrease, an indication of RGC, at T<900K, Fig. 4b and 5b. At higher pressure, a change in gradient reactivity is more pronounced, Fig.4b. This "slowdown" in ignition delay time gradient is caused by the three main competitive reaction pathways: the high-temperature formation of olefins and β-scission products; the chain branching peroxy- and hydroperoxy-radical reactions; and the cyclohexanone and bicyclic ethers ($cyC_6H_{10}Oa,b,c,d$) production. The reaction flux diagrams, Figure 6, indicate quite clearly these three pathways.

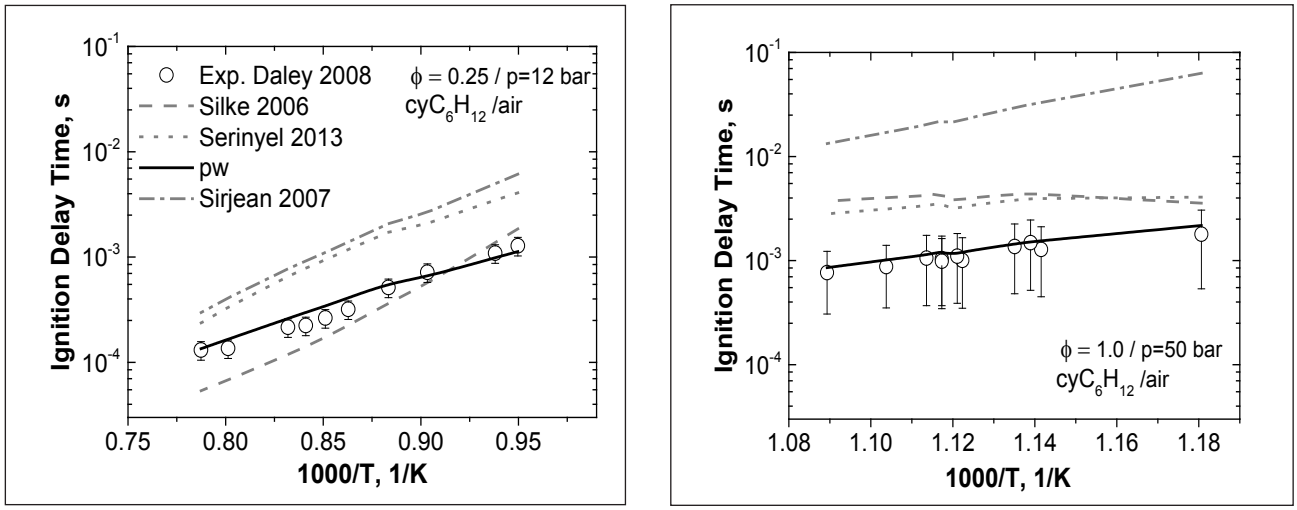

(a) (b)

Figure 4 – Comparison of ST autoignition data [16] with simulations [6, 8, 10], pw at: a) φ=0.25 , p=12bar; b) φ=1.0, p=50bar

At the low-temperature oxidation regime, Fig.6a, the cyclo-ketohydroperoxide chain-branching reaction path (starts with reaction type 12, see Figure 2) dominates and competes with the $cyC_6H_{10}Oa,b,c,d$ /chain-propagation paths (starts with reaction type 11, Figure 2).

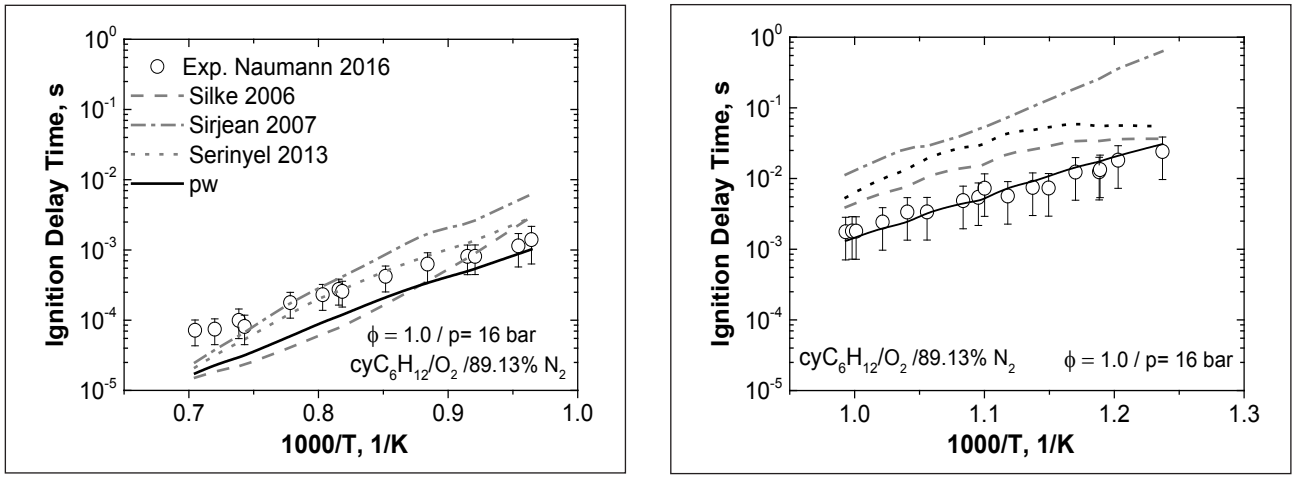

(a) (b)

Figure 5 – Comparison of ST autoignition data [22] with simulations [6, 8, 10], pw at: a)T=800-1010K b)T=1030-1420K

The new added reaction pathway, starting with cyC_6H_9OO formation (type 20, Figure2), influences the overall reaction for both temperature regimes, Fig.6a,b. It was pointed out that with the temperature increase the equilibrium constant of reaction $cyC_6H_{10}OOH \leftrightarrows cyC_6H_{10} + HO_2$ is shifted to the left side. It leads to the chain-propagation of cyclohexanone and bicyclic ethers, but not olefins and HO_2 radicals. As a consequence, cyclohexene starts two typical low-temperature scenarios, which prohibit the olefin accumulation and lead to the smoothed gradient change in the cyC_6H_{12} self-ignition behavior at 800 <T<1100K.

In both regimes, Fig.4 and 5, the experimental targets were perfectly regenerated by the current model. The models [8, 10] and of Sirjean et al. [6] overpre-

dict the ST ignition delay times and do not keep a trend. At higher temperature, T>900 K, models [6, 8, 10] are more successful by simulations, but tend to show a lower reactivity [6, 10]. It can be related to a) possible problems in thermodynamical properties; b) heightened concentrations of olefins, which should be produced in these models in large amount to reproduce the RCM experimental data [11, 17], Fig.3.

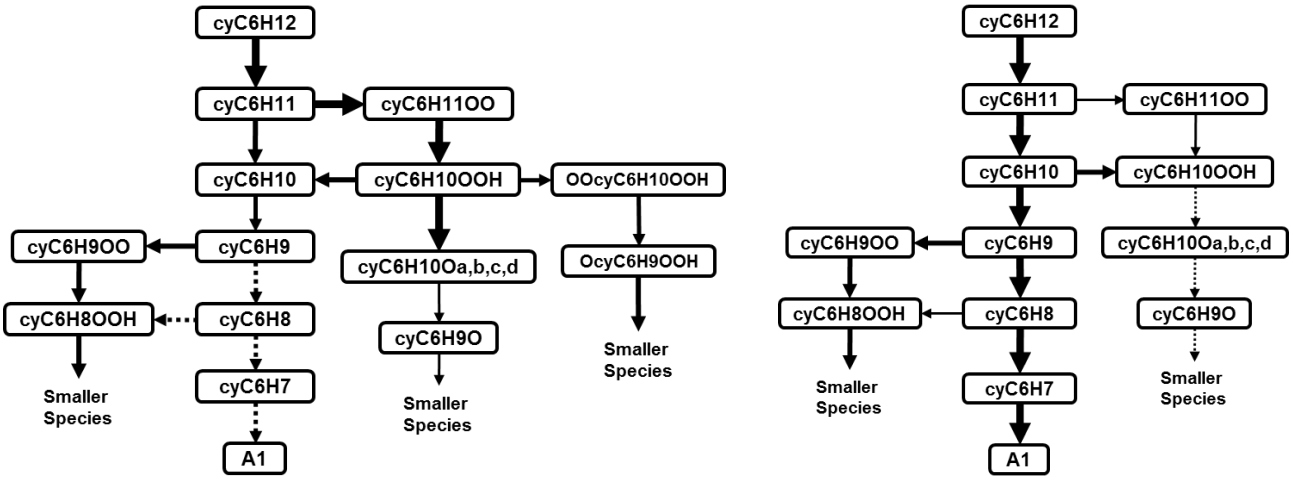

Figure 6 – Rate of production analysis in p = 16 atm and a) T=808 K and b) T=1389K

Laminar flame speed

The current mechanism has been also validated on the flame speed data from [10, 14, 15, 21]. The model demonstrates a good facilities to reflect the heat release in the system, describes datasets at atmospheric pressure and different preheated temperatures with a good agreement, Figure 7.

Flame structure

Figures 8 and 9 show simulations of the stabilized flames studied by Law et al. [13] and Ciajolo et al. [20]. In both cases the concentration profiles of important precursors of the PAH were successfully predicted with the present model.

The sensitivity and rate of production analysis have been carried out at three different temperatures along the given temperature profiles. It can be pointed out, that for T <1600K, the cascading dehydrogenation is the main reaction path to the benzene formation. The secondary ways lead to the substituted mono-aromatics after fuel decomposition to allene and acetylene. At the temperatures > 1600K, at the end of main reaction zone, the propargyl recombination controls the process of benzene formation, Figure 10.

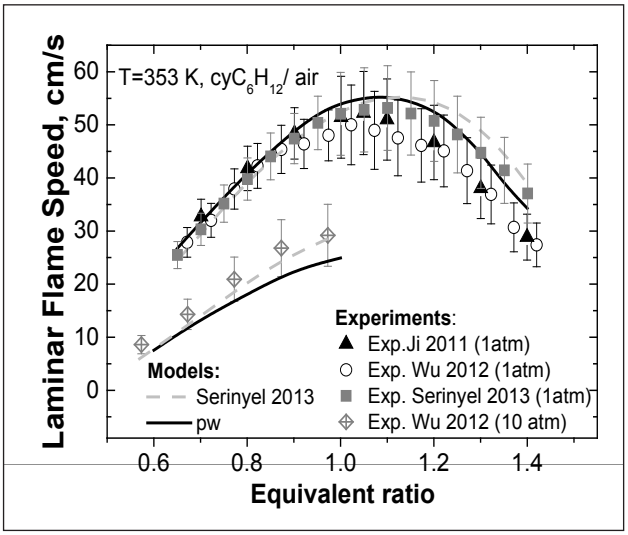

Figure 7 – Laminar flame speed data [10, 14, 15] compared with simulations [10],pw

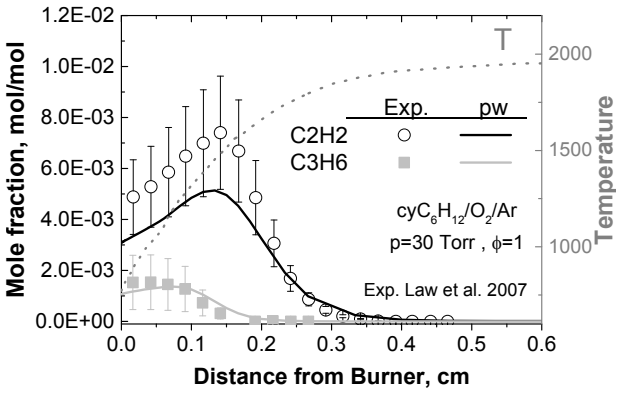

(a)

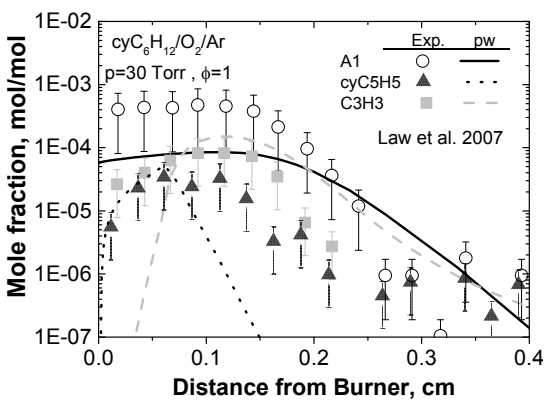

(b)

Figure 8 – Species concentration profiles reported by [13] and the simulation results [pw]

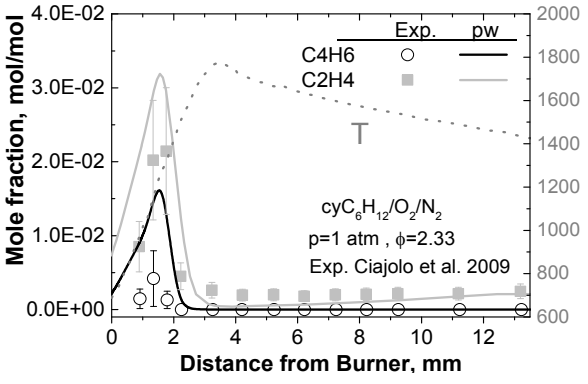

(a)

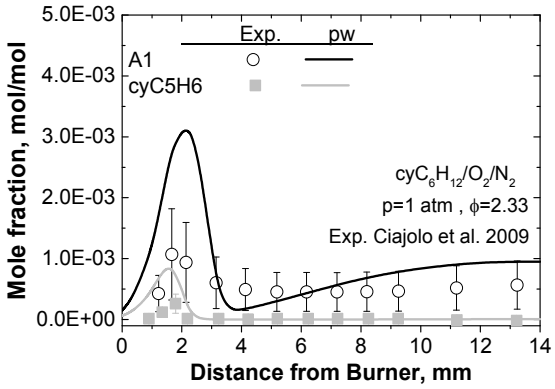

(b)

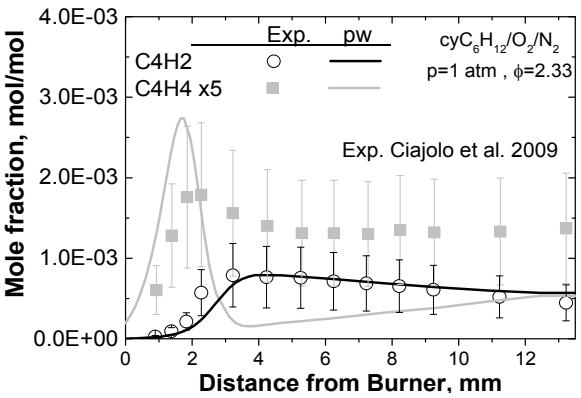

(c)

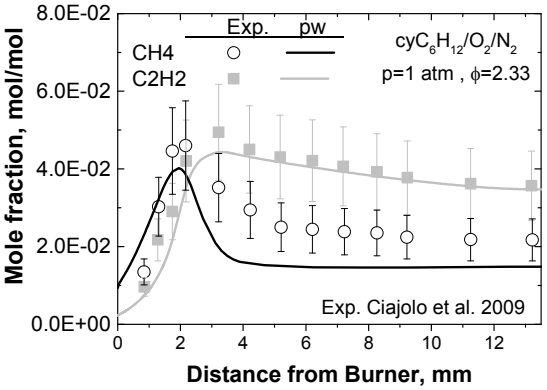

(d)

Figure 9 – Species concentration profiles reported by [20] and the simulation results [pw]

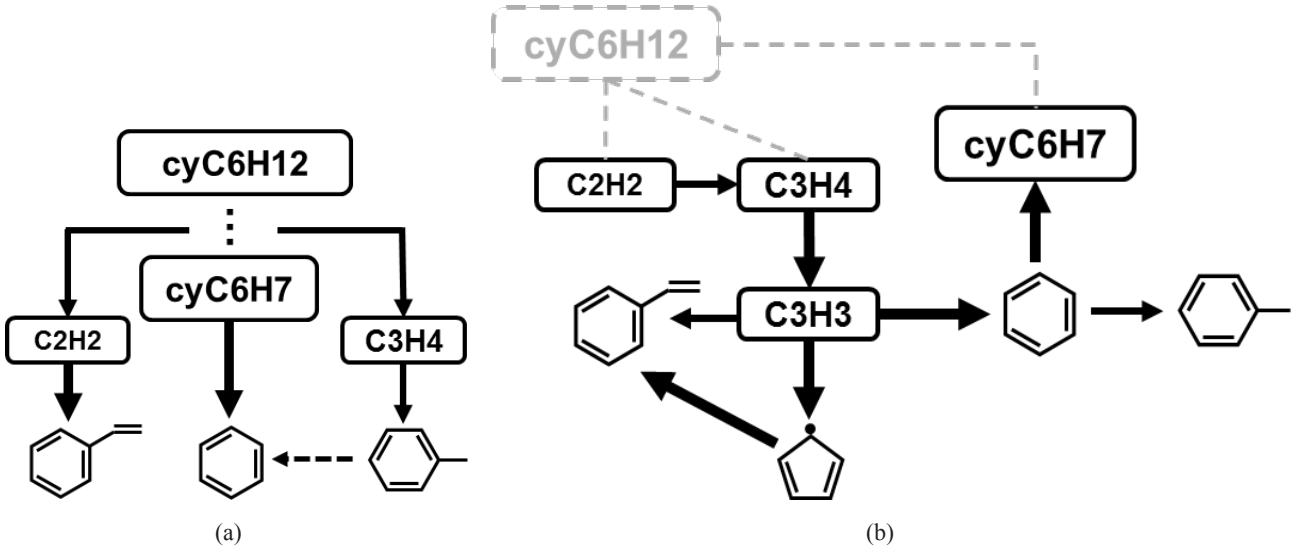

Figure 10 – Schematics of reaction path analysis performed for studied flames at a) temperature flame <1600K and b) temperature flame >1600K

4. Conclusions

This paper presents an updated semi-detailed kinetic mechanism for the cyclohexane oxidation at low, intermediate and high temperature. Two low-temperature reaction paths were newly included in the model: cyclohexenyl peroxy formation and isomerization of hydroperoxy peroxy radical. Special care has been taken to revise of rate parameters specific to cyclic alkanes and to evaluation of uncertainty intervals for the rate coefficients of most important reactions. The developed model satisfactorily reproduces the experimental data for ignition delay times, laminar flame speeds and concentration profiles measured in laminar flames. That makes it the particularly valuable for an explanation of the cyclohexane kinetics.

The equilibrium in the reaction of oxygen addition to cyC_6H_{11} is shifted to cyclohexyl peroxide production on the whole investigated temperatures interval, where three main competitive reaction pathways permanently control the ignition: the high-temperature formation of olefins and β-scission products; the chain branching peroxy- and hydroperoxy-radical reactions; and the cyclohexanone and bicyclic ethers production. The ignition simulations, thermochemistry, flow-rate and sensitivity analyses shown, that the competition of these three paths leads to the smoothed conversion of the high-temperature oxidation to the low-temperature. As the result, instead two stage ignition regime, the region of the gradient change (RGC) in the ignition behavior is occurred at 800<T<1100 K as a response to an increase of overall reactivity initiated by dominance of the chain branching peroxy- and hydroperoxy-radical reactions. Our numerical simulations are in accordance with the shock tube observations and support this conclusion. Further investigation of this matter would be very useful for the development of kinetic mechanisms for larger substituted naphthenes.

For T <1600K, the cascading dehydrogenation is the main reaction path to the benzene formation. The secondary ways lead to the substituted mono-aromatics after fuel decomposition to allene and acetylene. At the T > 1600K, the propargyl recombination controls the process of benzene formation.

References

1 D. Voisin, A. Marchal, M. Reuillon, J.-C. Boettner. Experimental and kinetic modeling study of cyclohexane oxidation in a JSR at high pressure // Combustion Science and Technology. – 1998. – Vol. 138. – P. 137-158

2 El Bakali, M. Braun-Unkhoff, P. Dagaut, P. Frank, M. Cathonnet. Detailed kinetic reaction mechanism for cyclohexane oxidation at pressure up to ten atmospheres // Proceedings of the Combustion Institute. – 2000. –Vol. 28. – P. 1631-1638.

3 Ristori, P. Dagaut, A. El Bakali, M. Cathonnet. The oxidation of n-propylcyclohexane: experimental results and kinetic modeling // Combustion Science and Technology. – 2001. – Vol. 165. – P. 197-228.

4 S. Granata, T. Faravelli, E. Ranzi. A wide range kinetic modeling study of the pyrolysis and combustion of naphthenes // Combustion and Flame. – 2003. – Vol. 132. – P. 533-544.

5 H. R. Zhang, L. Huynh, N. Kungwan, Z. Yang, S. Zhang. Combustion modeling and kinetic rate calculations for a stoichiometric cyclohexane flame.1. Major reaction pathways // J. Phys. Chem. A. – 2007. – Vol. 111. – P. 4102-4115.

6 Sirjean, F. Buda, H. Hakka, P. Glaude, R. Fournet, V. Warth, F. Battin-Leclerc, M. R. Lopez. The autoignition of cyclopentane and cyclohexane in a shock tube // Proceedings of the Combustion Institute. – 2007. – Vol. 31. – P. 277-284.

7 Cavallotti, R. Rota, T. Faravelli, E. Ranzi. Ab initio evaluation of primary cyclo-hexane oxidation reaction rates // Proceedings of the Combustion Institute. – 2007. – Vol. 31.– P. 201-209.

8 J. Silke, W. J. Pitz, C. K. Westbrook, M. Ribaucour. Detailed chemical kinetic modeling of cyclohexane oxidation // J. Phys. Chem. A. – 2007. – Vol. 111.– P. 3761-3775.

9 Buda, B. Heyberger, R. Fournet, P. Glaude, V. Warth, F. Battin-Leclerc. Modeling of the gas-phase oxidation of cyclohexane // Energy & Fuels. – 2006. – Vol. 20. – P. 1450-1459.

10 Z. Serinyel, O. Herbinet, O. Frottier, P. Dirrenberger, V. Warth, P. Glaude, F. Battin-Leclerc. An experimental and modeling study of the low- and high-temperature oxidation of cyclohexane // Combustion and Flame. – 2013. – Vol. 160. – P. 2319-2332.

11 O. Lemaire, M. Ribaucour, M. Carlier, R. Minetti. The production of benzene in the low-temperature oxidation of cyclohexane, cyclohexene, and cyclohexa-1,3-diene // Combust and Flame. – 2001. – Vol. 127.– P. 1971-1980.

12 S. G. Davis and C. K. Law. Determination of and fuel structure effects on laminar flame speeds of C1 to C8 hydrocarbons // Combustion Science and Technology. – 1998. – Vol. 140. – P. 427-449.

13 M. E. Law, P. R. Westmoreland, T. A. Cool, J. Wang, N. Hansen and T. Kasper. Benzene precursors and formation routes in a stoichiometric cyclohexane flame // Proceedings of the Combustion Institute. – 2007. – Vol. 31. – P. 565-573.

14 C. Ji, E. Dames, B. Sirjean, H. Wang and F. Egolfopoulos. An experimental and modeling study of the propagation of cyclohexane and mono-alkylated cyclohexane flames // Proceedings of the Combustion Institute. – 2011. – Vol. 33. – P. 971-978.

15 Wu, A. Kelley and C. Law. Laminar flame speeds of cyclohexane and mono-alkylated cyclohexanes at elevated pressures // Combust and Flame. – 2012. – Vol. 159. – P. 1417-1425.

16 S. Daley, A. Berkowitz and M. Oehlschlaeger. A shock tube study of cyclopentane and cyclohexane ignition at elevated pressures // International Journal of Chemical Kinetics. – 2008. – Vol. 40. – P. 624–634.

17 S. Vranckx, C. Lee, H. Chakravarty and R. Fernandes. A rapid compression machine study of the low temperature combustion of cyclohexane at elevated pressures // Proceedings of combuston institute. – 2012. – Vol. 34. – P. 377-384.

18 Z. Hong, K.-Y. Lam, D. Davidson and R.K. Hanson. A comparative study of the oxidation characteristics of cyclohexane, methylcyclohexane, and n-butylcyclohexane at high temperatures // Combust. Flame. – 2011. – Vol. 158. – P. 1456-1468.

19 S. Zeppieri, K. Brezinsky and I. Glassman. Pyrolysis studies of methylcyclohexane and oxidation studies of methylcyclohexane and methylcyclohexane/toluene blends // Combustion and Flame. – 1997. – Vol. 108. – P. 266-286.

20 Ciajolo, A. Tergrossi, M. Mallardo, T. Faravelli and E. Ranzi. Experimental and kinetic modeling study of sooting atmospheric-pressure cyclohexane flame // Proceedings of the Combustion Institute. – 2009. – Vol. 32. – P. 585-591.

21 S. Richter, M. B. Raida, C. Naumann and U. Riedel. Measurement of the laminar burning velocity of neat jet fuel components // Proceedings of the World Congress on Momentum, Heat and Mass Transfer (MHMT'16). – 2016. – Vol. 115. – P. 1-5.

22 C. Naumann and e. al. InnoTreib – innovative treibstoffe der zukunft // Bundesministerium für Wirtschaft und Energie (BMWi) Interim reports AP 4.2 and AP 6. – 2016.

23 M. Abbasi, N. A. Slavinskaya, U. Riedel. Kinetic modeling of cyclohexane oxidation including PAH formation // Proc. of 55th AIAA Aerospice sciences meeting 08.-13.01.2017. Grapevine, TX, USA – 2017, -P. 0838.

24 N. Slavinskaya, U. Riedel, S. Dworkin, M. Thomson. Detailed numerical modelling of PAH formation and growth in non-premixed ethylene and ethane flames // Combust. Flame. – 2011. – Vol. 159. -No.57. -Pp. 979-995.

25 N. A. Slavinskaya, M. Abbasi, J. H. Starcke, R. Whitside, A. Mirzayeva, U. Riedel, W. Li, J. Oreluk, A. Hegde, A. Packard, M. Frenklach, G. Gerasimov and O. Shatalov. Development of an UQ-predictive chemical reaction model for syngas combustion // Energy&Fuels. – 2016. – Vol. 3. – P. 2274-2297.

26 N.A.Slavinskaya, V. Chernov, R. Whitside, J.H. Starke, A. Mirzayeva, M. Abassi, M. Auyelkhankyzy. A modeling study of acetylene oxidation and pyrolisys // Combustion and Flame (submitted).

27 S. Benson. Thermochemical kinetics // 2nd ed., New Yorck, USA: John Wiley & Sons Ltd. – 1976.

28 K. Joback, R. Reid. Estimation of pure-component properties from group-contributions // Chemical Engineering Communications. – 1987. – Vol. 57. – P. 233-243.

29 R. Kee, F. Rupley, J. A. Miller. Sandia Laboratories Report, Sandia National Laboratories, Albuquerque, NM, 1993.

30 "Chemical Work Bench, Software Package, Ver. 4.1," Kintech Lab, Ltd., [Online]. Available: http://www.kintechlab.com/products/chemical-workbench. [Accessed 2017].

31 B. Sirjean, P. A. Glaude, M. F. Ruiz-Lopez and R. Fournet. Theoretical kinetic study of thermal unimolecular decomposition of cyclic alkyl radicals // J. Phys. Chem. A.– 2008. – Vol. 112. – P. 11598-11610.

32 Dayma, P. A. Glaude, R. Fournet, F. Battin-Leclerc. Experimental and modeling study of the oxidation of cyclohexene // International Journal of Chemical Kinetics. – 2003. – Vol. 7. – P. 273-285.

33 Y. Zhorov. Thermodynamics of chemical processes, petrochemical, synthesis, processing of petroleum, coal and natural gas // 1 ed., Moscow, Russia: Mir. – 1987. – P. 248.

34 M. Trautz, Z. Anorg. Evaluation of Arrhenius frequency factor (A) by simple collision theory // Chemistry. –1916. – Vol. 1. –P.1.

35 Chernyi, S. Losev, S. Macheret, B. Potapkin. Physical and chemical processes in gas dynamics : cross sections and rate constants: American institute of aeronautics & astronautics // AIAA. – 2012.

36 C. K. Westbrook, J. Warnatz and W. Pitz. A detailed chemical kinetic reaction mechanism for the oxidation of iso-octane and n-heptane over an extended temperature range and its application to analysis of engine knock // Proc. Combust. Inst. – 1989. – Vol. 22. – P. 893-901.

37 W. J. Pitz, C. Naik, T. Ní Mhaoldúin, C. Westbrook, H. J. Curran, J. Orme and J. M. Simmie. Modeling and experimental investigation of methylcyclohexane ignition in a rapid compression machine // Proc. Combust. Inst.– 2007. – Vol. 31. – P. 267-275.

38 E. Ranzi, T. Faravelli, P. Gaffuri and A. Sogaro. A wide-range modeling study of iso-octane oxidation // Combustion and Flame. – 1997. – Vol. 108. – P. 24-42.

39 Curran, P. Gaffuri, W. Pitz and C. Westbrook. A comprehensive modeling study of iso-octane oxidation // Combustion and Flame. – 2002. – Vol. 129. – P. 253-280.

40 D. Matheu, W. H. Green and J. Grenda. Capturing pressure-dependence in automated mechanism generation: reactions through cycloalkyl intermediates // Int. J. Chem. Kinet. – 2003. – Vol. 35. – P. 95.

41 V. Kurbatov und I. Silin. // Nuclear Instruments and Methods in Physics Reserach A, Bd. – 1994. – Vol. 345. – P. 346-350.

Supplementary Materials 1

Table S1 – Kinetic mechanisms and their experimental validations [1-20] (ST = Shock tube, RCM = Rapid Compression Machine, PFR = Plug Flow Reactor, JSR = Jet Stirred Reactor)

Model	Validation				
	ST	**RCM**	**PFR**	**JSR**	**Flame Structure**
Voisin et al. [1]				**Concentration profile [1]** **T=** 750-1100 K, **τ** =0.5 s **p=** 10atm, **φ=**0.5, 1.0, 1.5 **Mixture:** 0.1% cyC_6H_{12}/ O_2/N_2	
El Bakali et al. [2]				**Concentration profile [2]** **T=** 750-1200 K, **τ** =0.07-0.5 s **p=** 1, 2, 10atm, **φ=**0.5, 1.0, 1.5 **Mixture:** 0.15% $cyC_6H_{12}/O_2/N_2$	**Flame Speed [12]** **T=** 298 K **,** **p=** 1atm **Mixture:** cyC_6H_{12}/ air
Ristori et al. [3]				**Concentration profile [3]** **T=** 980-1200 K **p=** 1atm, **φ=**1.0, **τ** =0.07 s **Mixture:** 0.15% $cyC_6H_{12}/O_2/N_2$	
Granata et al. [4]		**Ignition delay time [11]** **p=** 7-9 bar **T=** 650-900 K **, φ=**1.0 **Mixture:** cyC_6H_{12}/ air	**Concentration profile [19]** **T=** 1155 K**, P=** 1atm **Mixture (pyrolysis):** 0.166 %cyC_7H_{14} in N_2 **T=** 1160 K**, p=** 1atm **Mixture:** 0.185% cyC_7H_{14}/1.9% O_2 in N_2	**Concentration profile [1,2]** **T=** 800-1200 K **P=** 1-10atm**,** **φ=**0.5, 1.0, 1.5	**Flame Speed [12]** **T=** 298 K **, p=** 1atm **Mixture:** cyC_6H_{12}/ air
Zhang et al. [5]					**Concentration profile [13]** **T=** 1000 K**,** **p=** 30 Torr **φ=**1.0, 2.0
Sirjean et al. [6]	**Ignition delay time [6]** **T=** 1200-1850 K **P=** 7-9 bar , **φ=**0.5, 1, 2 **Mixture:** 0.5% cyC_6H_{12}/O_2/Ar				

Cavallotti et al. [7]		**Ignition delay time [11]** **p**= 7-9, 11-14 bar **T**= 700-1000 K, **φ**=1.0 **Mixture:** cyC_6H_{12}/ air		**Concentration profile [2]** **T**= 800-1200 K **p**= 1-10atm , **φ**=0.5, 1.0, 1.5	
Silke et al. [8]		**Ignition delay time [11]** **p**= 7-9, 11-14 bar **T**= 700-1000 K, **φ**=1.0 **Mixture:** cyC_6H_{12}/ air		**Concentration profile [1]** **T**= 850-1070 K **,** **P**= 2.0 ,10atm **φ** = 0.5, 1.0, 1.5, **τ** =0.5 s **Mixture:** 0 .1% $cyC_6H_{12}/O_2/N_2$ **Concentration profile [2]** **T**= 800-1100 K, **τ** =0.25 s **p**= 5atm, **φ**= 1.0 **Mixture:** 0.15% $cyC_6H_{12}/O_2/N_2$	
Buda et al.[9]		**Ignition delay time [11]** **p**= 0.7-0.9/ 1.1-1.4 MPa **T**= 700-1000 K, **φ**=1.0 **Mixture :** cyC_6H_{12}/ air		**Concentration profile [1]** **T**= 850-1070 K , **p**= 10atm **φ** = 0.5, 1.0, 1.5 , **τ** =0.5 s **Mixture:** 0.1% $cyC_6H_{12}/O_2/N_2$	
Serinyel et al. [10]	**Ignition delay time [5]** **T**= 1200-1850 K **p**= 7-9bar, **φ**=0.5, 1, 2 **Mixture :** 0.5% cyC_6H_{12}/O_2 in Ar **Ignition delay time [17]** **T**= 950-1200 K **p**= 13-15 bar, **φ**=0.5, 1.0 **Mixture:** cyC_6H_{12}/ air **Ignition delay time [19]** **T**= 950-1200 K **p**= 1.5,3 bar, **φ**=0.5, 1.0 **Mixture :** $cyC_6H_{12}/4\%O_2/Ar$	**Ignition delay time [11]** **p**=11-14 bar **T**= 700-1000 K, **φ**=1.0 **Mixture:** cyC_6H_{12}/ air **Ignition delay time [18]** **T**= 600-900K, **φ** = 0.5,1,2 **p** = 12.5, 20, 40 bar **Mixture:** 2.26% $cyC_6H_{12}/O_2/N_2$		**Concentration profile [10]** **T**= 500-1100 K **P**= 1.07 bar , **τ** = 2 s **φ** = 0.5,1.0,2 **Mixture :** 0.667% $cyC_6H_{12}/O_2/N_2$	**Flame Speed [10]** **T**= 298,358, 398 K **p**= 1atm, **Mixture:** cyC_6H_{12}/ air **Flame Speed [12]** **T**= 298 K , **p**= 1atm **Mixture:** cyC_6H_{12}/ air **Flame Speed [14]** **T**= 353 K , **p**= 1atm **Mixture:** cyC_6H_{12}/ air **Flame Speed [15]** **T**= 353 K , **p**= 2,5, 10atm **Mixture:** cyC_6H_{12}/ air

Table S2 – Thermodynamic properties of cyclohexane relevant sub-model species

Species	ΔH^0_f / kJ·mol^{-1}	S^0 / J·mol^{-1}·K^{-1}	$C_p(T)$ /J·mol^{-1}·K^{-1})						
			300	**400**	**500**	**600**	**800**	**1000**	**1500**
cyC_6H_{11}	54.71	314.94	108.93	151.45	187.74	219.29	269.63	303.40	351.87
cyC_6H_{10}	-2.43	312.26	104.90	145.14	178.48	206.48	249.21	278.78	322.94
$cyC_6H_{11}O$	-68.23	331.55	119.54	165.33	204.39	238.41	292.65	327.12	377.29
$cyC_6H_{11}OO$	-83.07	365.14	128.43	175.69	216.32	251.33	305.45	341.77	401.12
$cyC_6H_{10}OOH$	-37.22	398.44	146.93	196.34	236.73	271.05	325.60	361.62	413.25
$cyOOC_6H_{10}OOH$	-179.92	441.33	162.45	214.36	256.87	292.58	347.54	382.68	443.32
$cyOOHC_6H_9OOH$	-136.14	472.73	168.99	218.78	260.29	295.34	349.00	393.86	430.91
$cyOC_6H_9OOH$	-332.26	410.57	150.61	197.32	233.21	263.51	314.66	346.45	404.90
cyC_6H_9OO	35.52	373.69	122.98	165.82	201.03	230.15	273.21	302.46	352.99
cyC_6H_8OOH	26.75	376.78	136.64	180.67	214.31	241.36	282.46	308.52	348.41
a-$cyC_6H_{10}O$	-125.81	284.42	118.94	163.80	201.43	232.90	279.48	311.26	369.62
b-$cyC_6H_{10}O$	-140.38	258.55	115.32	158.71	197.13	229.69	276.23	308.84	368.45
c-$cyC_6H_{10}O$	-220.08	227.65	111.26	155.67	194.99	228.12	274.82	307.84	367.71
d-$cyC_6H_{10}O$	-235.41	334.39	116.59	158.66	192.67	222.26	272.58	305.52	362.85
cyC_6H_9	131.45	313.62	97.80	132.26	163.44	190.17	228.81	257.17	298.06
cyC_6H_8	134.28	274.10	75.33	102.35	126.05	145.68	172.49	191.92	219.07
cyC_6H_7	200.56	305.77	97.56	129.46	156.63	178.98	210.14	232.58	263.86

Table S4 – Experimental data used for validations

Exp.	Validation		
	ST	**RCM**	**Flame Structure**
Law et al. [13]			**Concentration profile** **T=** 1000 K**, p=** 30 Torr**, φ=**1.0 **Mixture:** cyC_6H_{12}/O_2 in 32.5% Ar **MFR**=0.00214 g.cm^{-2}.s^{-1} UNC: ±20 -50%
Vranckx et al. [17]		**Ignition delay time** **T=** 600-900 K, **φ** = 1.0, **p=** 20 bar **Mixture:** 2.26% $cyC_6H_{12}/O_2/N_2$ UNC: ±50% -70%	
Lemaire et al. [11]		**Ignition delay time** **p=** 8 bar, **T=** 650-900 K **, φ=**1.0 **Mixture:** cyC_6H_{12}/ air UNC: ±40% – 60%	

Sirjean et al.[6]	**Ignition delay time** **T=** 1230-1840 K**,** **P=** 8atm **, φ=**0.5, 2.0 **Mixture:** 0.5% cyC_6H_{12}/O_2/Ar UNC: ±30 – 40%		
Ciajolo et al. [20]			**Concentration profile** **T=** 700 K**, p=** 1 atm**, φ=**2.33 **Mixture:** cyC_6H_{12}/O_2/39.4% N_2 **MFR**=0.00283 $g.cm^{-2}.s^{-1}$ UNC: ±20 – 50%
Richter et al. [21]			**Flame Speed** **T=** 473 K**, p=** 1 atm **Mixture:** cyC_6H_{12}/ air UNC: ±10%
Naumann et al. [22]	**Ignition delay time** **T=** 800-1400 K**,** **p=** 16atm**, φ=**1.0 **Mixture:** cyC_6H_{12}/O_2/ 89% N_2 UNC: ±30 – 60%		
Daley et al. [16]	**Ignition delay time** **T=** 950-1200 K **p=** 13-15 bar, **φ=**0.25, 0.5, 1.0 **Mixture :** cyC_6H_{12}/ air UNC: ±20 – 40%		
Wu et al. [15]			**Flame Speed** **T=** 353 K **, p=** 1.0, 10 atm **Mixture:** cyC_6H_{12}/ air UNC: ±10% , ±20
Ji et al. [14]			**Flame Speed** **T=** 353 K **, p=** 1.0 atm **Mixture:** cyC_6H_{12}/ air UNC: ±10%
Serinyel et al. [10]			**Flame Speed** **T=** 358 K**, p=** 1atm, **Mixture:** cyC_6H_{12}/ air UNC: ±10%

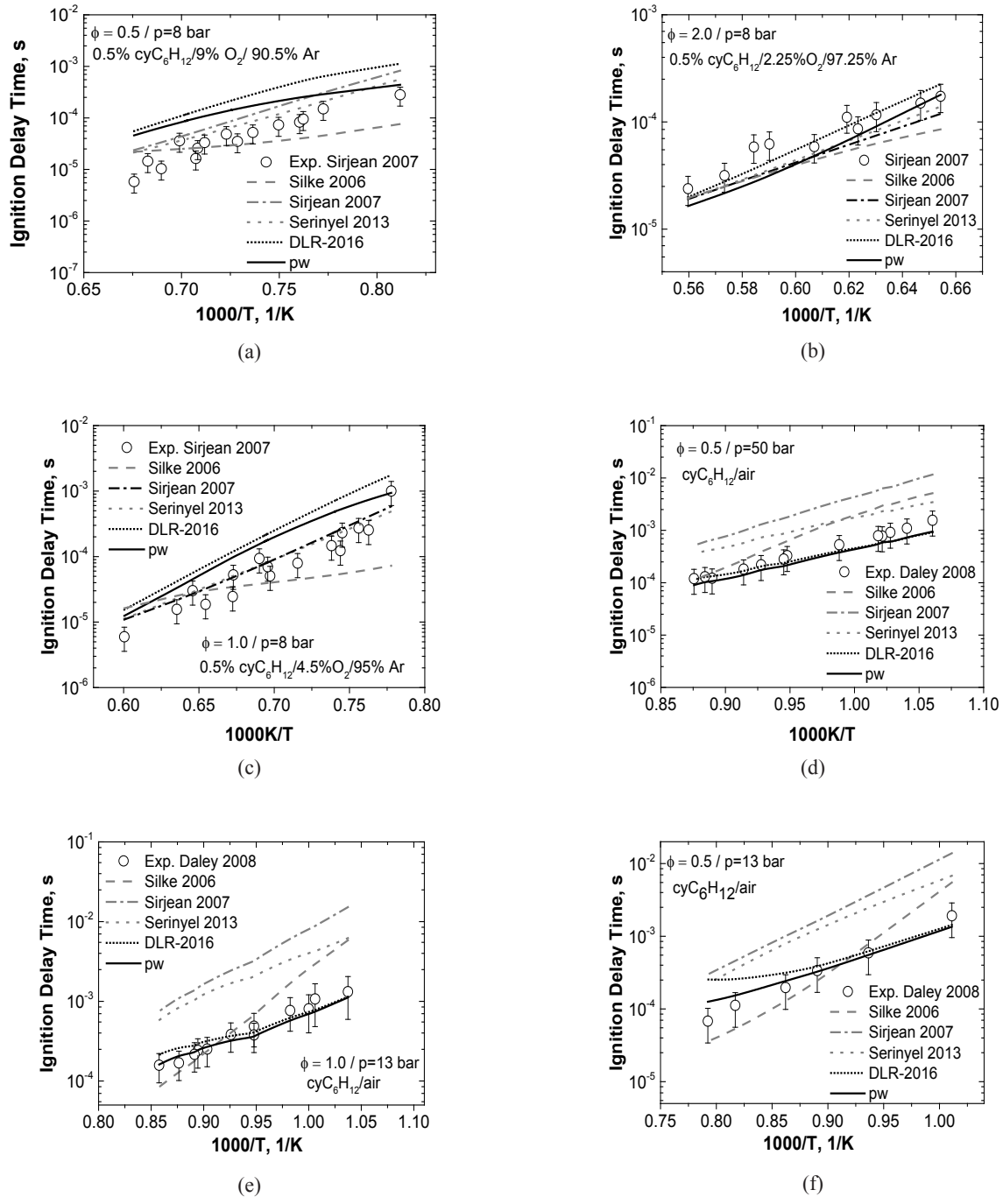

Figure S1 – Comparison of ST autoignition data [6,16] with simulations [6,8,10,23,pw]

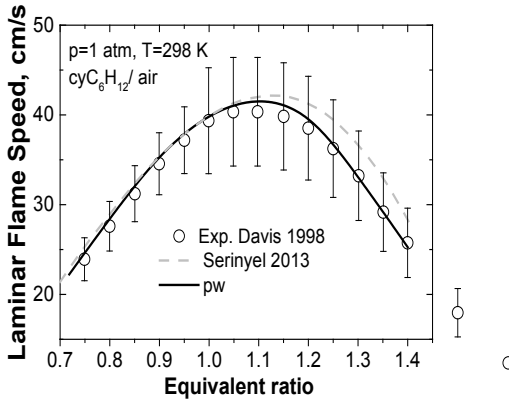

(a)

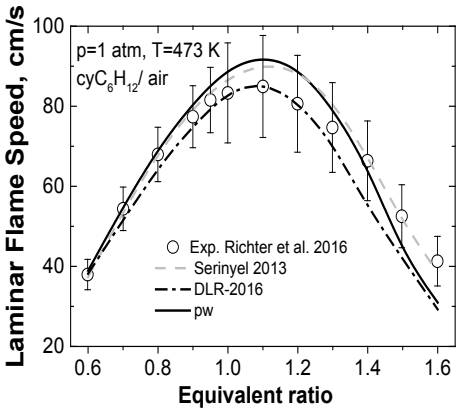

(b)

Figure S2 – Laminar flame speed data [12, 21] compared with simulations [10,23,pw].

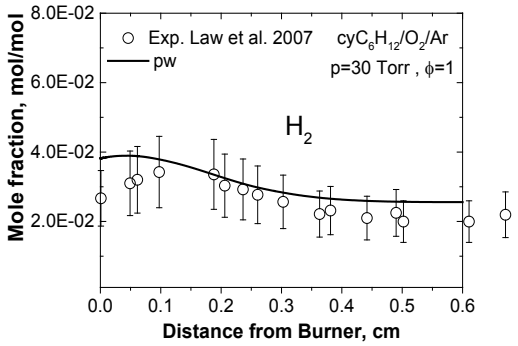

(a)

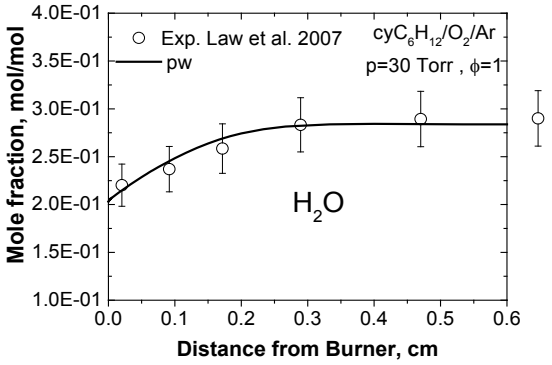

(b)

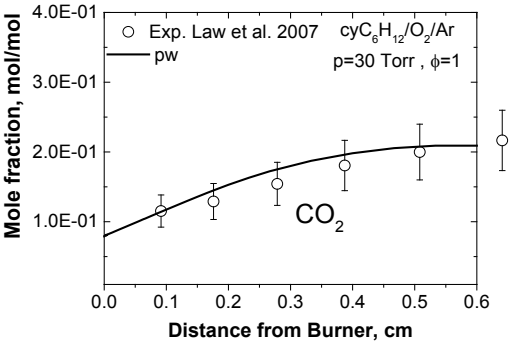

(c)

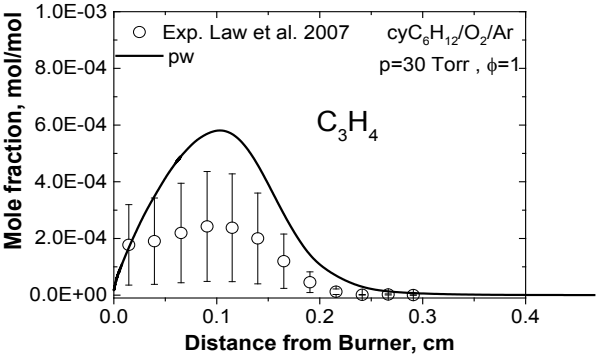

(d)

Figure S3 – Concentration profiles of species measured in burned stabilized flame of [13] and the simulation results [pw].

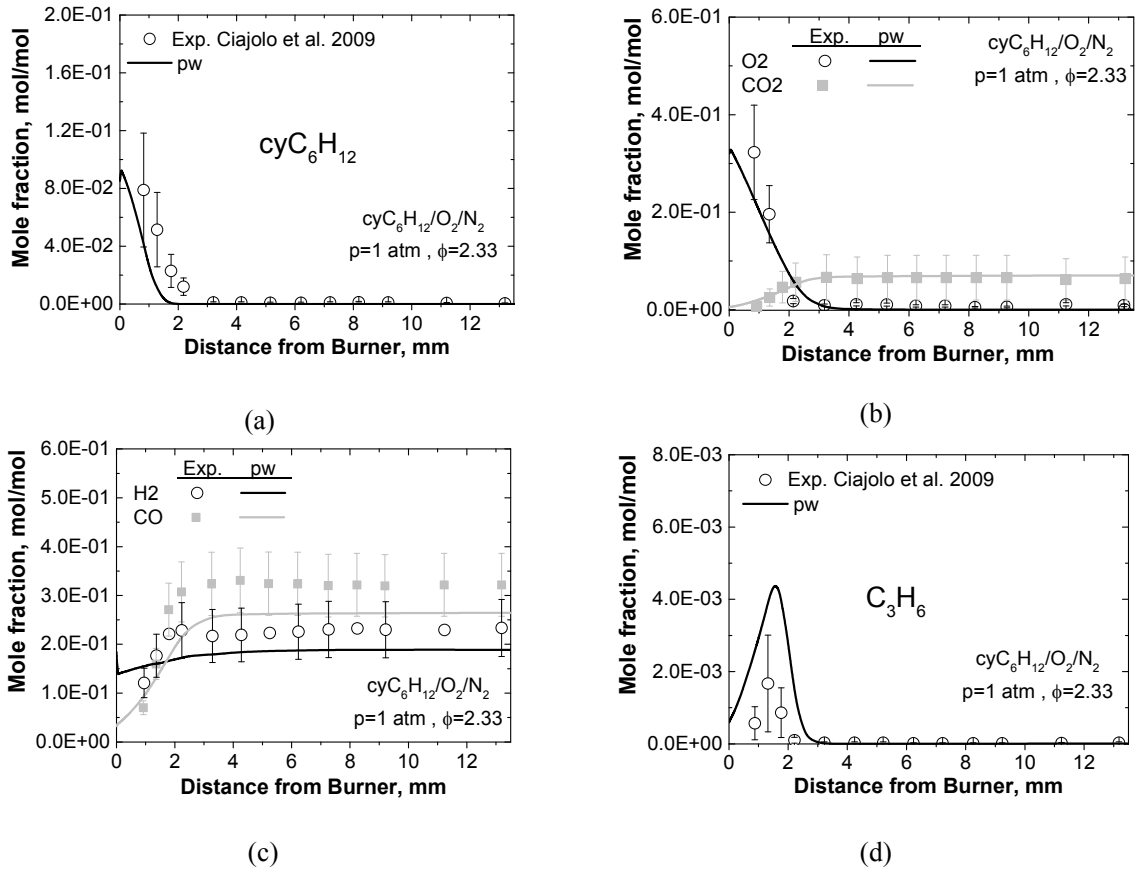

Figure S4 – Concentration profiles of species measured in burned stabilized flame of [20] and the simulation results [pw]

Supplementary Materials 2

Empirical rules for estimation of kinetic parameters of bi-molecular reactions:

The activation energy of a bi-molecular reaction can be approximated using the Polanyi-Semenov equations:

$$E_a = 48.1 - 0.25|\Delta H^0| \quad exothermic\ reactions \quad \text{Eq.(S1)}$$

$$E_a = 48.1 + 0.75|\Delta H^0| \quad endothermic\ reactions$$

where ΔH^0 is standard enthalpy of reaction. For reactions with two radicals as reactants, where the Polanyi-Semenov [1] equation results in negative values, the activation energy was assumed to be zero.

The pre-exponential factors were estimated based on the collision theory [2] using the numerical algorithm proposed in Cherny et al. [3].

Uncertainty analysis of the model rate parameters

Uncertainty of reaction model caused by mainly uncertainty of the chemical kinetics data (reaction rate coefficients, thermodynamic data, transport coefficients data, etc.) and experimental data which will be used for validation and optimization. In the case of the kinetic data, it is not simple to realize using of accurate first principle calculations for each reaction encountered in the kinetical model. The uncertainties for the published reaction rates are often not available or rarely reported [4]. The optimisation of kinetic model follows the reduction of model uncertainty. This could be achieved via minimizing the feasible area of parameters of reaction rate rule, in Arrhenius equation. The error margin for each reaction $\Delta k(T)$ included in the model is determined through the standard deviations of the rate coefficients A, n, E_a. The uncertainty factor $f(T)$ identifies the level of uncertainty of reactions. For lower and upper error boundaries, it will be defined as below [4]:

$$f_u(T) = log\frac{k_{upper}(T)}{k_0(T)}\ ,\ f_l(T) = log\frac{k(T)}{k_{low}(T)} \quad \text{Eq.(S2)}$$

where k_0 is the optimised rate value, known as nominal rate, k_{low} and k_{upper} are lower and upper rate boundaries. However, the statistical assessment of the rate is limited due to number of available data. If adequate sets of data are in access, the simple analysis of k uncertainty can be performed based on the least-squares regression. In this work the non-linear least squares method and its numeric realisation FUMILI [5]. It linearizes model $f(\vec{y},\vec{x})$ and approximates the goal function with modified parameters, which fits the data of m observations with a model of n unknown parameters ($m > n$).

The evaluation of parameters can be obtained through minimisation of objective function $\Phi(\vec{y},\vec{x})$ and linearization by a first-order Taylor series expansion about parameters:

$$\Phi(\vec{y},\vec{x}) = \sum_{j=1}^{m} \omega_j \left[Y_j^{exp} - \left(f_0(\vec{y},\vec{x}^*) + \sum_{k=1}^{n} \frac{\partial f_j(\vec{y},\vec{x})}{\partial x_k} \Delta x_k \right) \right]^2 \quad \text{Eq.(S3)}$$

The $\vec{y}$ is the vector of "coordinates", describing a physical property, such as temperature, pressure, etc. ; $\vec{x}$ is the vector of parameters to be modified, i.e. Arrhenius parameters A, n, and E_a in this case; ω_j is the weight of each set of observation, which directly correlates with experimental uncertainty and the Y_j^{exp} represents experimental set of data. Various sets of rate coefficients including experimental data, or literature data, by quantum chemistry or reaction models are assumed as statistical samplings (Y_j^{exp}). The weight coefficients are normally taken as claimed by the available literature sources. Otherwise an initial error equal to 50% will be prescribed to rate coefficients, which could be reduced or increased depending on the treatment process circumstances [4].

The vector of the parameter corrections Δx_k is obtained from n (from 1 to n_0) differential equations (for each parameter) following from minimisation of $\Phi(\vec{y},\vec{x})$:

$$\sum_{n=1}^{n_0} \left[\sum_{j=1}^{m} \omega_j \left(Y_j^{exp} - f_0(\vec{y},\vec{x}^*) \right) \frac{\partial f_j(\vec{y},\vec{x})}{\partial x_n} = \sum_{j=1}^{m} \omega_j \sum_{k=1}^{n} \frac{\partial f_j}{\partial x_k} \frac{\partial f_j}{\partial x_n} \Delta x_k \right] \quad \text{Eq.(S4)}$$

If we assign the derivative on the right side of the equation as $\Upsilon_{\alpha\beta}$, and on the left side of the equation as Ψ_{α}, as it comes in following (α,β: *1,..,*n_0):

$$\Upsilon_{\alpha\beta} = \sum_{j=1}^{m} \omega_j \frac{\partial f_j}{\partial x_\alpha}\frac{\partial f_j}{\partial x_\beta} \quad ,$$

$$\Psi_{\alpha} = \sum_{j=1}^{m} \omega_j \left(Y_j^{exp} - f_0(\vec{y},\vec{x}^*)\right)\frac{\partial f_j(\vec{y},\vec{x})}{\partial x_\alpha} \quad \text{Eq.(S5)}$$

Therefore, the vector Δx_k can be concluded as following:

$$\Delta x_k = \sum_{i=1}^{n} (\Upsilon^{-1})_{ki}\Psi_i \quad \text{Eq.(S6)}$$

The Υ^{-1} term is assigned as error (co-variance) matrix. This gives us information about parameters such as errors $s(x)$, and deviations of calculated functions (mean values of coefficients k_0), $\Delta f(\vec{y},\vec{x})$. These two are defined as following:

$$s(x_\alpha) = \left[\frac{v\varphi}{m-n} D(x_\alpha)\right]^{1/2},$$

$$f = t_s \left[\frac{\varphi}{m-n}\sum_{\alpha=1}^{n}\ \sum_{\beta=1}^{n}\left(\frac{\partial f}{\partial x_\alpha}\right)\left(\frac{\partial f}{\partial x_\beta}\right) cov(x_\alpha, x_\beta)\right]^{1/2}$$

Eq.(S7)

where φ is the sum of reduced deviations squares; $cov(x_\alpha, x_\beta)$ are the elements of the co-variance matrix $\Lambda\, D(x_\alpha) = \Lambda(x_{\alpha\alpha})$;the term $\left[\frac{\varphi}{m-n}\right]^{1/2}$ estimates the reduced standard deviation for the observations (experimental data); t_s is the coefficient of proportionality for $\Delta f/s(f)$ with a certain confidence probability [4].

The obtained Arrhenius parameters give the mean (nominal) values of the rate constant k_0. Therefore, with the approximated values of the errors vector $s(x_\alpha)$ from Eq.(S7), and the uncertainty degree of rate coefficient parameters, the lower and upper rate boundaries can be described as following:

$$k_{low}(T) = (A - s(A))T^{(n-s(n))}exp(-(E_a + s(E_a))/T)$$

Eq.(S8)

$$k_{upper}(T) = (A + s(A))T^{(n+s(n))}exp(-(E_a - s(E_a))/T)$$

The overall coefficients which characterize correlation of one parameter with others can be obtained via the co-variance matrix Λ as:

$$Q_\alpha = (1 - 1/R_\alpha)^{1/2},\ R_\alpha = \Lambda(x_{\alpha\alpha})\cdot\Lambda(x_{\alpha\alpha})^{-1} \quad \text{Eq.(S9)}$$

Also the pair correlation which characterizes the connection of parameters with each other is defined as below:

$$q_{\alpha\beta} = \frac{\Lambda(x_{\alpha\beta})}{(\Lambda(x_{\alpha\alpha})\cdot\Lambda(x_{\beta\beta}))^{1/2}} \quad \text{Eq.(S10)}$$

Table S3 – Reaction rate and estimated lower and upper uncertainty factors for modified reactions

Reaction*	ΔT, K	Initial rate [6]			Ref.	Modified rate			Ref.	f_l and f_u
		A	β	E_a		A	β	E_a		
$cyC_6H_{12} + O \leftrightarrows cyC_6H_{11} + OH$	500-3000	2.60E+06	2.0	2553	[7]	4.34E+09	1.33	3427.5	generic [a]	4.07-4.25
$cyC_6H_{11}+O_2 \leftrightarrows cyC_6H_{10}+HO_2$	700-3000	1.50E+12	0.0	4251.2	[8]	1.17E+13	0.0	7479.7	EM [b]	1.68-1.77
$cyC_6H_{10} + H \leftrightarrows cyC_6H_9 + H_2$	500-3000	3.97E+13	0.0	6562	EM	6.00E+12	0.0	4445	[9]	2.25-2.56
$cyC_6H_{10}+HO_2 \leftrightarrows cyC_6H_9+H_2O_2$	600-3000	1.14E+13	0.0	10709.5	EM	4.49E+10	0.6	15828	generic	2.39-2.61
$cyC_6H_{11}OO \leftrightarrows cyC_6H_{10}OOH$	800-3000	1.50E+12	0.0	24076	[10] [c]	2.00E+12	0.0	24045	[11] [d]	3.34-3.82
$cyC_6H_{10}OOH \leftrightarrows OH+cyC_6H_{10}Oa$	700-3000	1.00E+12	0.0	10400	[12]	9.31E+09	0.6	8437.08	generic	2.84-3.14
$cyC_6H_{10}OOH \leftrightarrows OH+cyC_6H_{10}Ob$	600-3000	1.50E+12	0.0	23400	[12]	1.25E+10	0.8	21662.2	generic	3.51-3.86
$cyC_6H_{10}OOH \leftrightarrows OH+cyC_6H_{10}Oc$	800-3000	1.90E+12	0.0	20700	[12]	1.08E+12	0.6	23692.3	generic	2.78-2.97

Notes: * Reaction rate constants in cm^3, mol, cal units, $k = AT^{\beta}exp(E/RT)$
a) Estimated average rate coefficients by uncertainty analysis (REAC-UQ) **b)** Estimated using the empirical method [1-3]
c) Analogous with C_8 **d)** The factor A multiplied by 2/3

1. Y. M. Zhorov, Thermodynamics of Chemical Processes; Petrochemical synthesis, processing of petroleum, coal, and natural gas, 1st Edition, Moscow, Russia: Mir Publications, 1987.

2. M. Trautz and Z. Anorg, "Evaluation of Arrhenius Frequency Factor (A) by Simple Collision Theory," Chemistry, vol. 1, 1916.

3. G. Chernyi, S. Losev, S. Macheret and B. Potapkin, Physical and Chemical Processes in Gas Dynamics : Cross Sections and Rate Constants: American Institute of Aeronautics & Astronautics, 20 Jun 2002., Reston, United States: AIAA, 2012.

4. Slavinskaya, N.A.; Chernov, V.; Whitside, R.;Starke, J.H.; Mirzayeva, A.; Abassi, M.; Auyelkhankyzy, M., „A modeling study of acetylene oxidation and pyrolisys," Combustion and Flame, submitted.

5. V. Kurbatov und I. Silin, *Nuclear Instruments and Methods in Physics Reserach A,* Bd. 345, pp. 346-350, 1994.

6. M. Abbasi, N. A. Slavinskaya and U. Riedel, "Kinetic Modeling of Cyclohexane Oxidation Including PAH Formation," Grapevine, Texas, USA, 2017.

7. A. Ristori, P. Dagaut, A. El Bakali and M. Cathonnet, "The Oxidation of N-Propylcyclohexane: Experimental Results and Kinetic Modeling," *Combustion Science and Technology,* pp. 197-228, 2001.

8. H. R. Zhang, L. Huynh, N. Kungwan, Z. Yang and S. Zhang, "Combustion Modeling and Kinetic Rate Calculations for a Stoichiometric Cyclohexane Flame.1. Major Reaction Pathways," *J. Phys. Chem. A,* pp. 4102-4115, 2007.

9. D. Voisin, A. Marchal, M. Reuillon and J.-C. Boettner, "Experimental and Kinetic Modeling Study of Cyclohexane Oxidation in a JSR at High Pressure," *Combustion Science and Technology,* vol. 138, pp. 137-158, 1998.

10. H. Curran, P. Gaffuri, W. Pitz and C. Westbrook, "A Comprehensive Modeling Study of iso-Octane Oxidation," *Combustion and Flame,* pp. 253-280, 2002.

11. Granata, S., Faravelli, T., Ranzi, E., "A wide range kinetic modeling study of the pyrolysis and combustion of naphthenes," Combustion and Flame, Vol. 132, 2003, pp. 533-544.

12. Silke, E. J., Pitz, W. J., Westbrook, C. K., Ribaucour, M., "Detailed Chemical Kinetic Modeling of Cyclohexane Oxidation," J. Phys. Chem. A, Vol. 111, 2007, pp. 3761-3775..